R. & M. No. 3623

MINISTRY OF TECHNOLOGY

AERONAUTICAL RESEARCH COUNCIL
REPORTS AND MEMORANDA

On Lifting Surfaces Supporting One or More Plane Shock Waves

By J. PIKE

Aerodynamics Dept., R.A.E., Bedford

LONDON: HER MAJESTY'S STATIONERY OFFICE
1970

PRICE £1 1*s* 0*d* [£1·05] NET

On Lifting Surfaces Supporting One or More Plane Shock Waves

By J. PIKE

Aerodynamics Dept., R.A.E., Bedford

Reports and Memoranda No. 3623*
April, 1966

Summary

Stream surfaces from the flow through a plane shock wave are used as compression surfaces to obtain high lift to drag ratios. The inviscid performance of these compression surfaces is known exactly, and at given values of M_∞ and C_L, higher values of L/D can be achieved than the two-dimensional wedge value. The improvement that can be obtained over this value depends on the similarity parameter $C_L^{\frac{1}{2}} M_\infty^2/\beta_\infty$ and is large when this parameter is small.

Two such compression surfaces can be combined into a W-Nonweiler shape, which gives in effect a central body below a swept wing. The viscous drag tends to be high, because the shapes have a large ratio of wetted area to plan area. For hypersonic speeds ($M > 5$) where the inviscid improvement over a two-dimensional wedge is small, the high viscous drag puts the W-wings at a disadvantage compared with flat-bottomed configurations (though not as compared with caret wings). At high supersonic speeds ($3 < M < 5$) the inviscid improvement is more marked and a gain in performance, including viscosity, over that of the two-dimensional wedge, and hence over that of flat-bottomed shapes can be shown. Such conclusions do not take into account the relative problems of converting idealised shapes into practical aircraft configurations.

For best performance the trailing edge of the W-wing is swept and its pressure drag and viscous drag are approximately equal.

*Replaces R.A.E. Technical Report 66 127—A.R.C. 28 452.

LIST OF CONTENTS

1. *Introduction*

Caret wings[1,2] have been used as typical non-slender or 'waverider' shapes for aerodynamic calculations at high supersonic and hypersonic speeds[3]. The caret wing (Fig. 1(a)) is a wing of delta planform the undersurface of which conforms to streamlines of the flow behind a plane inclined shock wave. Assuming a streamwise upper surface and neglecting base drag, the inviscid performance (i.e. lift/drag ratio) is the same as that of a plane two-dimension wedge and hence it depends only on two variables, say the free stream Mach number and pressure coefficient. Even when more general planforms are included, the performance is still that of the wedge provided the leading edge remains in the plane shock wave, and the trailing edge is not so highly swept as to cause breakdown in the parallel flow over the surface.

The caret wing has a plane shock wave which is inclined in the flow so as to deflect the air vertically downwards. This same shock wave with a different orientation can give the deflected air a sideways component of velocity. Shapes the same as caret wings, associated with these skew shock waves, are called 'V'-wings in this Report. It is shown that with the correct trailing edge, the V-wing can have a very much better performance than the caret wing.

Two V-wings can be joined along part of their leading edges to form a 'W-Nonweiler' wing or 'W'-wing. A W-wing of gothic planform is shown in Fig. 1b. The consideration of viscous drag calls for W-wings with curved leading edges. These are referred to as generalised W-wings. Their performance, including an estimate for viscous drag, is compared with that of a two-dimensional wedge at the same lift coefficient.

A special case of the W-wing has been investigated by Roe[4]. He compares the 'direct' lift of a caret wing, with the 'interference' lift of a vertical unswept wedge below a plane wing of particular planform. The direct lift of the caret may be compared immediately with the lift due to incidence of a two-dimensional wedge, the flow adjacent to the surface in both cases having been deflected vertically down by the shock wave (Fig. 2a). The lift of the interference wing is the result of the pressure field of the vertical wedge acting on the plane wing. The flow adjacent to the wing is deflected horizontally by the shock wave (Fig. 2b). For values of a parameter $M_\infty^4 \, C_L/\beta_\infty^2 < 0{\cdot}65$ the interference arrangement has better performance than the caret wing, and *vice-versa* above this value[4]. A performance better than either could possibly be produced by a combination of 'direct' and 'interference' lift. A way of obtaining this with a wing based on the flow through a plane shock wave, is to orientate the shock wave so that the flow deflection lies in a plane between the vertical and horizontal. This can give a W-wing as shown in Fig. 2c. The ratio of interference to direct lift may then be conveniently defined as the tangent of the angle that this plane makes with the vertical.

A previous paper on caret and W-wings has been presented by Keldysh[5]. He uses a different approach, applicable only to wings with straight leading edges. Unfortunately he omits to restrict the trailing edge to maintain the 'local' flow direction over the whole surface, and thereby, it is considered, obtains an over-estimate of the optimum performance.

The use of inclined shock waves can produce a variety of configurations with straight and curved surfaces. It emerges that those of 'optimum' performance have a deep central body beneath an arrow wing. The improvement in inviscid performance over that of the caret wing at high supersonic speeds ($3 < M < 5$ say) is considerable, and even at hypersonic speeds as $M \to \infty$ it can be as much as 8 per cent. The inclusion of viscous drag reduces the advantage these wings have over the two-dimensional wedge, so that at hypersonic speeds it is no longer advantageous to use interference methods. It is shown that the optimum L/D at high supersonic speeds is obtained when the viscous drag is of about the same magnitude as the pressure drag.

The shapes evolved here do not have sufficient latitude to allow practical aircraft configurations to be specified in detail. However it is hoped that they provide a guide to the arrangement and shape of wing and fuselage necessary to obtain the advantages of favourable interference at high supersonic speeds.

2. *Compression Surfaces Based on the Flow Through an Oblique Shock Wave.*

The compression surface of a generalised V-wing (e.g. Fig. 3) possesses the following properties:

(a) the leading edge lies on a plane inclined shock wave;

(b) the surface is formed from straight generators, parallel to the flow immediately behind the shock wave (i.e. the surface has single curvature);

(c) the trailing edge is supersonic.

These properties imply that the leading edge is supersonic, and that between the surface and the shock wave, (neglecting viscous effects), the flow is parallel and the pressure and other flow parameters are constant. A supersonic trailing edge requires that the influence of any point on the trailing edge should not affect the flow at any other trailing-edge point. Hence the trailing edge remains in the region of parallel flow. With supersonic leading and trailing edges the flow over the compression surface is independent of the other surfaces which form the wing. Hence its performance may be considered independently from the other surfaces, or taken to represent that of a wing with a streamwise upper surface and zero base drag.

For the caret wing, the deflection through the shock wave is vertical. For V-wings the deflection is allowed to take place in other planes and two or more such compression surfaces may be joined with a common leading edge to give a more complex wing shape. Generalised W-wings are formed from a mirror image pair of these compression surfaces (e.g. Fig. 1b). The performance is, of course, the same as that of either of the pair, and hence W-wings are included in the following analysis on generalised V-wings.

Let x, y, z be stream axes (Fig. 1a), where x is in the free stream flow direction and z is vertically downwards. Also let the reference area of the force coefficients be the plan area, shown in Fig. 4, i.e.

$$A_z = \int_S \mathbf{z}_0 \,.\, \mathbf{dS} \tag{1}$$

where $\mathbf{S}$ is the compression surface, $\mathbf{dS}$ an element of $\mathbf{S}$ with its normal into the flow behind the shock wave, and $\mathbf{z}$ is unit vector parallel to the $\mathbf{z}$ axis. The pressure is constant over $\mathbf{S}$, hence the lift coefficient based on A_{z_0} is

$$C_L = C_p \tag{2}$$

where C_p is the pressure coefficient behind the shock wave. This implies that the centre of pressure is coincident with the centre of area.

If we define the free stream Mach number and lift-coefficient, equation (2) gives C_p, and the oblique shock wave relationships[6] are sufficient to give the shock wave inclination to the x-axis (σ), the flow deflection through the shock wave (δ) and all other flow parameters in the region of parallel flow.

Throughout Sections 2 to 5 of this Report C_L and M_∞ will be taken as fundamental and specified. Although σ and δ are then prescribed, their orientation to the y and z-axes is still arbitrary. One further parameter is necessary to fix the orientation. This is defined by letting the flow deflection take place in a plane which makes an angle λ with the x, z-plane. This plane is perpendicular to the shock wave, and the shock wave equation can be written as

$$z \cos\lambda + y \sin\lambda = x \tan\sigma \,. \tag{3}$$

With this notation, the ratio of 'direct' lift to 'interference' lift proposed in the introduction is given by $\tan\lambda$. With $\lambda = \pi/2$ the lift is all interference lift and the wings become 'wedge-interference' wings[4]. With $\lambda = 0$ the lift is all 'direct', and the inviscid performance is equivalent to that of the caret wing.

If (C_{Dp}, C_S, C_L) are the inviscid force coefficients in the $x, y, -z$ directions, and if suffix $(\,)_0$ refers to the wing with $\lambda = 0$, then

where

$$\begin{cases} C_{Dpo} = C_p \tan \delta \\ C_{So} = C_p \tan \xi \\ \tan \xi = -A_{yo}/A_{zo} \\ C_{Lo} = C_p \end{cases} \tag{4}$$

where A_{zo} is A_z for the wing when $\lambda = 0$ (as in Fig. 4), and A_{yo} is defined similarly to A_{zo} i.e. by

$$A_{yo} = \int_S \mathbf{y} \,.\, \mathbf{dS} \qquad \text{with } \lambda = 0 \,. \tag{5}$$

Hence $\tan \xi$ depends only on the geometry of the surface. As the pressure over the surface is constant ξ is related to the force coefficients by equations (4)
i.e.

$$\tan \xi = C_{So}/C_{Lo} \,. \tag{6}$$

The angle ξ is also the angle between the vectors $y\,C_S + z\,C_L$ and the vertical z-axis. The value of ξ is restricted physically to lie between certain limits which will be determined in the next Section.

The lift to drag ratio can be obtained from equation (4) and the oblique shock wave relationships[6]. For $\lambda = 0$,

$$\left(\frac{L}{D_p}\right)_o = \cot \delta = \frac{2 - C_p}{C_p \cot \sigma} \tag{7}$$

$$= \frac{2 - C_L}{C_L} \left(\frac{4 + (\gamma+1)\, C_L\, M_\infty^2}{4\,\beta_\infty^2 - (\gamma+1)\, C_L\, M_\infty^2} \right)^{\frac{1}{2}} . \tag{8}$$

This is shown as C_L^2/C_{Dpo} *versus* C_L in Fig. 5.

For $\lambda \neq 0$ the force coefficients are obtained in terms of those of equations (4) by

$$C_{Dp} = \frac{A_{zo}}{A_z} C_{Dpo} \tag{9a}$$

$$C_S = \frac{A_{zo}}{A_z} (C_{So} \cos \lambda - C_{Lo} \sin \lambda) \tag{9b}$$

$$C_L = \frac{A_{zo}}{A_z} (C_{Lo} \cos \lambda + C_{So} \sin \lambda) \,. \tag{9c}$$

Combining equations (2), (4) and (9c):

$$\frac{A_{zo}}{A_z} = \frac{1}{\cos \lambda + \tan \xi \sin \lambda} = \frac{\cos \xi}{\cos (\xi - \lambda)} \tag{10}$$

and equations (9) may be rewritten

$$\left.\begin{aligned} C_{Dp} &= C_p \tan\delta \frac{\cos\xi}{\cos(\xi-\lambda)} \\ C_S &= C_p \tan(\xi-\lambda) \\ C_L &= C_p . \end{aligned}\right\} \tag{11}$$

These equations are the force coefficients of the generalised V-wing. Assuming that M_∞ and C_L are given, they depend on λ and ξ only. The function of these which appears in the drag is fundamental to the performance, for

$$\frac{\cos\xi}{\cos(\xi-\lambda)} = \frac{C_{Dp}}{C_p \tan\delta} = \frac{C_{Dp}}{C_{Dpo}} = \frac{(L/D_p)_o}{L/D_p} . \tag{12}$$

This is plotted against $\tan\xi$ for various λ in Fig. 6. C_L is a constant for the Figure and $\cos\xi/\cos(\xi-\lambda)$ represents an increase or decrease in C_D compared with the caret wing value ($\lambda = 0$). The envelope of the curves gives the minimum value of C_D/C_{Do}. Hence only when $\xi = 0$ does $\lambda = 0$ give the most efficient wing. $\xi = 0$ is equivalent to $A_{yo} = 0$ and hence is the value of ξ for an unswept trailing edge* (x = constant). For $\xi \neq 0$, $L/D > (L/D)_0$ when $0 < \lambda < 2\xi$. Further $\lambda = \xi$ gives the maximum value of L/D_p
i.e.

$$(L/D_p)_{\max} = (L/D_p)_o \sec\xi = \cot\delta \sec\xi \tag{13}$$

and

$$C_S = 0 . \tag{14}$$

Thus for a given geometry (i.e. given ξ) the optimum non-viscous performance is obtained by arranging for a ratio of interference lift to direct lift equal to $\tan\xi$. The overall force on the surface then acts in the vertical x, z-plane ($C_S = 0$). This implies that the overall momentum change also takes place vertically. The local momentum change through the shock wave (due to δ), takes place at angle λ to the vertical. It is converted to a vertical momentum change by the flow in the wake. Roe[4] using his particular 'W'-wings noted that 'near field' momentum considerations, used for example by Eggers and Syvertson[7], could be misleading. They assume that the near-field momentum change for an efficient wing should be vertical. This, as applied to W-wings (by putting $\lambda = 0$), only gives the most efficient wing when $\xi = 0$; that is when there are no prospects of improving the performance by interference.

3. *The Geometry of Wings with their Trailing Edges Lying in a Plane.*

3.1. *Theory.*

A natural set of axes with which to investigate the geometry of generalised V-wings (i.e. with shock wave skew) are rectangular axes (X, Y, Z) with X streamwise behind the shock wave, Y in the plane of the shock wave and Z on the free stream side of the wave (*see* Fig. 3). When $\lambda = 0$ these axes (i.e. X_o, Y_o, Z_o) are related to the (x, y, z) axes by a rotation δ about the $y = Y_o$ axis
i.e.

$$\left.\begin{aligned} x &= X_o \cos\delta - Z_o \sin\delta \\ y &= Y_o \\ z &= X_o \sin\delta + Z_o \cos\delta . \end{aligned}\right\} \tag{15}$$

*ξ is zero also for any wing where the trailing edge projects onto a single line in a plane perpendicular to the shock wave containing the x-axis.

The X, Y, Z axes are fixed with respect to the shock wave, hence for $\lambda \neq 0$ a rotation λ about the x-axis followed by a rotation δ about the y-axis relates to two sets of axes. Hence

$$\left.\begin{aligned} x &= X\cos\delta - Z\sin\delta \\ y &= X\sin\delta\sin\lambda + Y\cos\lambda + Z\cos\delta\sin\lambda \\ z &= X\sin\delta\cos\lambda - Y\sin\lambda + Z\cos\delta\cos\lambda. \end{aligned}\right\} \tag{16}$$

The equation of the general compression surface in X, Y, Z co-ordinates is given by

$$f(Y,Z) = 0\,. \tag{17}$$

It is bounded upstream by the shock wave with equation

$$X = BZ \qquad \text{where } B = \cot(\sigma - \delta) \tag{18}$$

and downstream by the trailing edge. The trailing edge is for simplicity restricted to lie in a plane, hereafter called the trailing-edge plane, with equation

$$X + aY + bZ = c \tag{19}$$

where a, b and c are constants. For any trailing edge on a particular trailing-edge plane the value of ξ is constant. This can be seen to be true by considering an elemental streamtube, when the relative contributions to $A_{yo}\,(= A_Y)$ and $A_{zo}\,(= A_Z \sec\delta)$ are independent of the streamtube chosen. Hence the proportions are constant for any bundle of such streamtubes, that is for any wing. The result is derived in Appendix A, along with the further result that the maximum value of ξ can be obtained using a plane trailing-edge surface.

To aid the discussion we define the nose (*see* Fig. 7) as P_1 $(0, 0, 0)$, the wing tips as P_2 (X_2, Y_2, Z_2) and P_3 (X_3, Y_3, Z_3) on the intersection of the trailing-edge plane and shock wave, and the intersection of the nose streamline with the trailing-edge plane as P_4 $(X_4, 0, 0)$. The trailing-edge plane is fully determined by P_2, P_3 and P_4. Hence given these, the value of ξ is fixed, and so it may be evaluated by considering *any* wing with its trailing edge on this plane. In particular we choose the wing with straight leading and trailing edges through P_1, P_2, P_3 and P_4 as shown in Fig. 7. It can be seen that

$$\tan\xi = -\frac{A_{yo}}{A_{zo}} = \frac{Z_3 - Z_2}{(Y_3 - Y_2)\cos\delta}. \tag{20}$$

Using equation (18) this becomes

$$\tan\xi = \frac{X_3 - X_2}{(Y_3 - Y_2)\,B\cos\delta} \tag{21}$$

Hence ξ depends on P_2 and P_3 only, and is therefore constant for any trailing edge on any trailing-edge plane through P_2, P_3.

In the previous section the trailing edge was required to be supersonic (condition 'c' of the generalised V-wing). We shall restrict the trailing-edge plane such that any trailing edge on it will be supersonic. This requires that the downstream Mach cone from any point on the trailing-edge plane shall not intersect the plane,
i.e.

$$\left(\frac{\partial X}{\partial Y}\right)^2 + \left(\frac{\partial X}{\partial Z}\right)^2 \geqslant \beta^2\,. \tag{22}$$

Hence, using equation (19)

$$a^2+b^2 \geqslant \beta^2 . \tag{23}$$

Substituting the co-ordinates of $P_4\,(X_4, 0, 0)$ in equation (19) we have

$$X_4 = c \tag{24}$$

hence equation (23) will restrict the value of X_4 as follows. P_2 and P_3 satisfy equation (19) hence

$$(X_3-X_2)+a\,(Y_3-Y_2)+b\,(Z_3-Z_2) = 0 . \tag{25}$$

Then using equation (20) and (21) to substitute for (Z_3-Z_2) and (X_3-X_2) this becomes

$$a+b\tan\xi\cos\delta+B\tan\xi\cos\delta = 0 .$$

Further using equations (18) and (19) with $c = X_4$ (equation (24)) we have

$$\frac{-a}{B\tan\xi\cos\delta} = 1+\frac{b}{B} = \frac{X_4}{X_2-Y_2\,B\tan\xi\cos\delta} . \tag{26}$$

Equation (23) can then be written

$$a^2+\left(B+\frac{a}{\tan\xi\cos\delta}\right)^2 \geqslant \beta^2 . \tag{27}$$

Hence, 'a' lies between the roots p_1, p_2 of the quadratic equation

$$p^2\,(1+\tan^2\xi\cos^2\delta)+2\,p\,B\tan\xi\cos\delta+(B^2-\beta^2)\tan^2\xi\cos^2\delta = 0 . \tag{28}$$

That is between the values

$$\frac{-B\tan\xi\cos\delta}{1+\tan^2\xi\cos^2\delta}\left\{1\pm\left[1\pm\left(1-\frac{\beta^2}{B^2}\right)\left(1+\tan^2\xi\cos^2\delta\right)\right]^{\frac{1}{2}}\right\} . \tag{29}$$

From equation (26), limits on X_4 are given by

$$\frac{X_2-Y_2\,B\tan\xi\cos\delta}{1+\tan^2\xi\cos^2\delta}\left\{1\pm\left[1-\left(1-\frac{\beta^2}{B^2}\right)\left(1+\tan^2\xi\cos^2\delta\right)\right]^{\frac{1}{2}}\right\} . \tag{30}$$

Hence the range of X_4 is restricted for a particular P_2 and ξ (or P_3 using equation (21)). X_4 influences the sweep of the trailing edge (*see* Fig. 7). The minimum trailing-edge sweep for a W-wing is given by the upper limiting value of X_4.

The equation of $P_2\,P_3$ is given by the intersection of the trailing-edge plane (equation (19)) with the shock wave (equation (18)),

i.e.

$$X = BZ = \frac{aB}{b+B}\left(\frac{c}{a}-Y\right). \tag{31}$$

This line is used in constructing configurations to have specified values of ξ and λ, that is with a particular performance. In x, y, z co-orinates it becomes.

$$\frac{y_3-y_2}{x_3-x_2} = \frac{\tan\sigma-\tan\delta}{\tan\xi}\cos\lambda+\tan\sigma\sin\lambda \tag{32}$$

$$\frac{z_3-z_2}{x_3-x_2} = \tan\sigma\cos\lambda-\sin\lambda\frac{\tan\sigma-\tan\delta}{\tan\xi}. \tag{33}$$

When $\lambda = \lambda_{opt} = \xi$ these reduce to

$$\frac{y_3-y_2}{x_3-x_2} = \frac{\tan\sigma-\cos^2\xi\tan\delta}{\sin\xi} \tag{34}$$

$$\frac{z_3-z_2}{x_3-x_2} = \cos\xi\tan\delta. \tag{35}$$

As the left hand sides of these equations (32) to (35) depend on differences between x_2, y_2, z_2 and x_3, y_3, z_3 respectively, only the relative positions of P_2 and P_3 are determined. Hence it is always possible to arrange for $y_2 = 0$, the condition, along with P_1 P_2 being a straight line, that a mirror image pair will form a W-wing. Hence equations (34) and (35) enable W-wings with a particular C_L (giving σ and δ through equations (7) and (8)) and a particular L/D (giving ξ from equation (11)) to be constructed easily. If $\lambda \neq \xi$ equations (32) and (33) should be used.

3.2. *Examples.*

Some examples of W-wings are shown in Fig. 8. Those of Fig. 8a and 8b are wings at $M = 2$ with the same shock wave and trailing-edge surface, such that $\lambda = \xi = \pi/4$. X_4 is at its maximum limit in both cases. Other values of X_4 would shorten the distance $P_1 P_4$, giving greater trailing-edge sweep and a relatively deeper body.

Although the wings of Figs. 8a and 8b look very different, their only real difference is in scale and the position of P_3 on the line given by equations (34) and (35). By varying the position of P_3 on this line, intermediate values of trailing-edge sweep can be obtained at intermediate values of anhedral. The anhedral can be varied with little difference to the performance by varying λ such that $\cos(\xi-\lambda)$ (*see* equation 11)) is little different from unity.

The equation of the leading edge of the body is given by putting $y = 0$ in equation (3),

i.e.
$$z\cos\lambda = x\tan\sigma. \tag{36}$$

Hence the inclination to the free stream increases with λ and with σ. At higher Mach numbers the body will tend to be more highly swept.

In Fig. 8c a W-wing at $M = 4$ is shown, with the same value of $\lambda = \xi = \pi/4$. The body is more highly swept, and compared with Fig. 8b so are the leading and trailing edges.

A compression surface at $M = 10$ is shown in Fig. 8d.

More interesting shapes can be obtained with curved leading edges. Fig. 9a shows a wing with turned down tips and Fig. 9b a wing with a curved surface.

The examples given in Figs. 8 and 9 are in themselves far removed from being realistic shapes for aircraft. However by introducing some modifications, progress can be made towards more practical configurations. Two possibilities are presented in Figs. 10 and 11. In Fig. 10 two compression surfaces similar to those of Fig. 9a are arranged astride a long thin fuselage. The effect of the nose shock wave from the fuselage will be small and make little difference to the performance of the compression surfaces. The wing tips can be modified as in Fig. 10, with only a small change in the performance. The compression surfaces C_L remains the same, but the C_D is increased (3 per cent in Fig. 10) owing to the change in reference area. A more significant change is of course the inclusion of a large viscous drag term from the body. Viscous effects are considered in Section 6.

To introduce the examples shown in Fig. 11 it is recalled that the trailing edges of all these W-wings have been restricted to lie within the region of known flow. If the trailing edge is modified so as to permit a region over which the pressures are not precisely known, then the body length can be extended or the trailing-edge sweep reduced to produce a more realistic configuration. A first example is included in Fig. 8c where an extension to the body (the dashed line) increases the volume while making little difference to the performance excluding viscosity, (for evaluation of the volume *see* Appendix 2).

In Fig. 11, a more extensive region has been added, constituting 30 per cent of the plan area. The design Mach number is 4 and the C_p for the known part is 0·0691. Hence the known part contributes 0·0484 to the overall lift coefficient. The inviscid drag from this lift is 80 per cent of that from a similar C_p on a caret wing. The lift and drag of the added region are not known. The C_p must be expected to be less than the known value, and the efficiency less than that of the caret wing. However a useful contribution to the performance can obviously be obtained from the region. For the performance quoted in Fig. 11, the pessimistic value of $C_p = 0$ has been used. It might be noted that the centre of pressure must be expected to be forward of the centre of area.

Some further variation of the surface shapes could be achieved by using wings based on the flow about curved two-dimensional wedges. The line $P_1 P_4$ then no longer remains straight, but may be curved to give more body volume forward. $(L/D_p)_o$ is no longer related to C_{Lo} by equation (8), but W wings may be formed in the same way from V wings. The performance of V wings from slightly curved wedges will be little different from those of plane wedges, but significantly curved wedges will tend to give inferior performance[8].

4. *Optimum Wings Neglecting Viscous Drag.*

Consider now wings with maximum L/D_p, with respect to ξ and λ. From equation (12) it can be seen that we require ξ to be a maximum and λ to equal ξ. As the class of plane trailing-edge surfaces includes the optimum surface (*see* Appendix A) we may restrict ourselves to plane surfaces. From equation (21), maximum ξ is given by maximum $(X_3-X_2)/(Y_3-Y_2)$. P_2 and P_3 lie on the shock wave, and for the maximum value of $(X_3-X_2)/(Y_3-Y_2)$, P_3 will lie on the down stream Mach cone of P_2. Then, using Fig. 12

$$\left(\frac{X_3-X_2}{Y_3-Y_2}\right)_{\max} = \frac{\beta B}{(B^2-\beta^2)^{\frac{1}{2}}} \tag{37}$$

and from equation (21)

$$\tan \xi_{\max} = \frac{\beta}{\cos\delta\,(B^2-\beta^2)^{\frac{1}{2}}}. \tag{38}$$

Then

$$1+\tan^2\xi\cos^2\delta = \frac{B^2}{B^2-\beta^2}. \tag{39}$$

From equation (29) the value of 'a' is unique and is given by

$$a = \frac{-B\tan\xi_{\max}\cos\delta}{1+\cos^2\delta\tan^2\xi_{\max}} \tag{40}$$

$$= -\beta\left(1-\frac{\beta^2}{B^2}\right)^{\frac{1}{2}} \tag{41}$$

Then the trailing edge plane from equations (19), (24), (26), (27), (38) and (41) is sonic and has equation

$$B(X-X_4)-\beta(B^2-\beta^2)^{\frac{1}{2}}\,Y-\beta^2\,Z=0\,. \tag{42}$$

The lift to drag ratio from equations (11) is

$$\frac{L}{D_p}=\cot\delta\frac{\cos(\xi-\lambda)}{\cos\xi}. \tag{43}$$

Using equation (38), for $\xi=\xi_{\max}$ in equation (43)

$$\frac{L}{D_p}=\frac{\cos\lambda\,(B^2-\beta^2)^{\frac{1}{2}}+\sin\lambda\,\beta\sec\delta}{\tan\delta\,(B^2-\beta^2)^{\frac{1}{2}}}. \tag{44}$$

With optimum λ also (i.e. $\lambda=\xi=\xi_{max}$)

$$\left(\frac{L}{D_p}\right)_{max}=\cot\delta\left(\frac{B^2+\beta^2\tan^2\delta}{B^2-\beta^2}\right)^{\frac{1}{2}}. \tag{45}$$

Equations (7), (8) and (45) are used to plot $(C_L^2/C_{Dp})_{max}$ for various free stream Mach numbers in Fig. 13. The caret wing value

$$\left(\frac{C_L^2}{C_D}\right)_o=\frac{C_L^2}{C_{Dpo}}=C_L\cot\delta \tag{46}$$

shown in Fig. 5, is also included for comparison. The optimum value is noticeably greater than the caret wing value at all C_L and M_∞, but strikingly so for small C_L and low M_∞ together. The singularity in $C_L^2/C_D\,(\xi=\xi_{\max})$ as $C_L\to 0$ is investigated by small disturbance theories in the next Section.

Keldysh in his paper[5] on V and W-wings with straight leading and trailing edges, in effect failed to consider the limits on ξ. Thus taking the equivalent of $\xi_{\max}=\pi/2$ instead of the value given by equation (38), he obtained $(L/D_p)_{\max}=\infty$.

5. *Small Disturbance Expressions.*

From Ref. 6

$$\frac{C_p}{2}=\frac{\delta}{\beta_\infty}-\left(1-\frac{\gamma+1}{4}\,\frac{M_\infty^2}{\beta_\infty^2}\right)\frac{\delta^2}{\beta_\infty^2}+0(\delta^3) \tag{47}$$

Hence, to first order

$$\left(\frac{L}{D}\right)_o=\cot\delta=\frac{2}{C_L\beta_\infty}\left(1-\frac{C_L}{2}+\frac{\gamma+1}{8}\,\frac{M_\infty^4}{\beta_\infty^2}C_L\right) \tag{48}$$

i.e.

$$\frac{\beta_\infty}{2}\left(\frac{C_L^2}{C_{Dp}}\right)_o = 1+\frac{M_\infty^4\, C_L}{8\,\beta_\infty^2}\left\{\gamma+\left(1-\frac{2}{M_\infty^2}\right)^2\right\} \tag{49}*$$

From equations (45) and (38),

$$\left(\frac{L}{D}\right)_{\max} = \cot\delta\left(\frac{B^2+\beta^2\tan^2\delta}{B^2-\beta^2}\right)^{\frac{1}{2}} \tag{50}$$

$$\tan\xi_{\max} = \frac{\beta}{\cos\delta\,(B^2-\beta^2)^{\frac{1}{2}}}. \tag{51}$$

From Ref. 4, or putting δ small in the oblique shock wave relationships

$$\beta-\beta_\infty = -\frac{M_\infty^2}{\beta_\infty^2}\left(1+\frac{\gamma-1}{2}M_\infty^2\right)\delta \tag{52}$$

and

$$B-\beta_\infty = \left(1-\frac{\gamma+1}{4}\frac{M_\infty^2}{\beta_\infty^2}\right)M_\infty^2\,\delta. \tag{53}$$

Hence, from equation (50)

$$\left(\frac{L}{D}\right)_{\max} = \frac{\beta_\infty}{\delta\,M_\infty^2}\left(\frac{2\,\beta_\infty}{(\gamma+1)\,\delta}\right)^{\frac{1}{2}} \tag{54}$$

---

*This equation is misquoted in Ref. 4.

and from (51)

$$\tan \xi_{\max} = \left(\frac{2\beta_\infty}{(\gamma+1)\delta} \right)^{\frac{1}{2}} \frac{\beta_\infty}{M_\infty^2}. \tag{55}$$

Equations (47) and (54) give

$$\frac{\beta_\infty}{2} \left(\frac{C_L^2}{C_{Dp}} \right)_{\max} = \left(\frac{4}{\gamma+1} \right)^{\frac{1}{2}} \Big/ \frac{M_\infty^2 C_L^{\frac{1}{2}}}{\beta_\infty} \tag{56}$$

and equation (55) shows $\xi_{\max} (= \lambda) \to \pi/2$. The parameter $M_\infty^2 C_L^{\frac{1}{2}}/\beta_\infty$ appeared in a logarithmic form in the performance of the wedge-interference wings ($\lambda = \pi/2$) of Ref. 4. Equation (56) gives the optimum small disturbance performance for wedge-interference wings, with a supersonic trailing edge. The exact performance, can of course be obtained by putting $\lambda = \pi/2$ in equations (43) and (44).

In Fig. 14, with $M_\infty^2 C_L^{\frac{1}{2}}/\beta_\infty$ as abscissa exact values of $(\beta_\infty/2)(C_L^2/C_{Dp})$ are compared with the small disturbance theory values. Agreement is good for small values of $M_\infty^2 C_L^{\frac{1}{2}}/\beta_\infty$. At larger values the exact performances are better than those predicted by small disturbance theory. As $C_p = C_L$ for all wings, the non-linearity in C_L can be removed by relating the performance to that of the caret wing ($\lambda = 0$). This is shown in Fig. 15, where the values of $(L/D_p)_{\max}/(L/D_p)_o$ for $M = 2, 4$ and 10, are in remarkable agreement at equivalent values of $M_\infty^2 C_L^{\frac{1}{2}}/\beta_\infty$. This obviously permits evaluation of the possible improvement in performance at other Mach numbers.

For $M_\infty^2 \delta$ large and δ small, the oblique shock wave relationships or Ref. 9 give

$$\left.\begin{aligned} C_p &= (\gamma+1)\delta^2 \\ B &= \frac{2}{(\gamma-1)\delta} \\ \beta &= \frac{1}{\delta}\left(\frac{2}{\gamma(\gamma-1)} \right)^{\frac{1}{2}}. \end{aligned}\right\} \tag{57}$$

Hence, substituting as before, we can obtain

$$\left.\begin{aligned}(C_L^2/C_{Dp})_o &= (\gamma+1)^{\frac{1}{2}}\, C_L^{\frac{1}{2}} \\ (C_L^2/C_{Dp})_{\max} &= (2\gamma)^{\frac{1}{2}}\, C_L^{\frac{1}{2}} \\ (L/D_p)_{\max}/(L/D_p)_o &= \left(\frac{2\gamma}{\gamma+1}\right)^{\frac{1}{2}}\end{aligned}\right\} \tag{58}$$

and

$$\tan \xi_{\max} = \left\{\frac{(\gamma-1)}{(\gamma+1)}\right\}^{\frac{1}{2}}.$$

For $\gamma > 1$, the improvement in performance does not disappear, as $M_\infty \to \infty$. For example with $\gamma = 1{\cdot}4$, $(L/D)_{\max}/(L/D)_o$ has a value of 1·08 and $\xi_{\max} = \lambda \sim 22°$. Hence the optimum ratio of 'interference' to 'direct' lift does not become zero even as $M_\infty \to \infty$. These limit values for large $M_\infty^2\, C_L^{\frac{1}{2}}/\beta_\infty$ are shown on Figs. 14 and 15.

6. *Performance Including Viscosity.*

Let C_f be an average skin-friction coefficient and S_w the wetted area of the lower surface, then

$$\left.\begin{aligned}C_X &= C_f\, S_w/A_Z \\ C_Y &= C_p \tan \xi \cos \delta \\ C_Z &= -C_p\end{aligned}\right\} \tag{59}$$

where C_X, C_Y, C_Z are force coefficients with A_Z as reference area. Since $A_{zo} = A_Z \cos \delta$, from equation (10) it follows that

$$A_z = A_Z \cos \delta \frac{\cos(\xi-\lambda)}{\cos \xi}. \tag{60}$$

Hence, using equations (16), (59) and (60), we can write

$$C_D = C_p \frac{\cos \xi}{\cos (\xi - \lambda)} \left\{ \tan \delta + \frac{C_f}{C_p} \frac{S_w}{A_Z} \right\} \tag{61}$$

$$= C_p \frac{\cos \xi}{\cos (\xi - \lambda)} \tan \delta + C_f \frac{S_w}{A_z} \cos \delta \tag{62}$$

$$C_S = C_p \tan (\xi - \lambda) + \sin \lambda \sin \delta \, C_f \frac{S_w}{A_z} \tag{63}$$

$$C_L = C_p - C_f \frac{S_w}{A_z} \sin \delta \cos \lambda \,. \tag{64}$$

When $C_f = 0$ these reduce to equations (11). Now $C_f \frac{S_w}{A_z} \sin \delta \cos \lambda < C_p$ and is neglected.
Then for the lower surface

$$\frac{L}{D} = \frac{\cos (\xi - \lambda) \sec \xi}{\tan \delta + \frac{C_f}{C_p} \frac{S_w}{A_z}} \tag{65}$$

and

$$\left(\frac{L}{D} \right)_o = \frac{1}{\tan \delta + \frac{C_f}{C_p} \frac{S_w}{A_z}} . \tag{66}$$

This may also be written as

$$\frac{L}{D} = \frac{C_L}{C_{Dp} + C_{Df}} \tag{67}$$

where $C_{Dp} = C_{Do} \frac{\cos \xi}{\cos (\xi - \lambda)}$ and $C_{Df} = C_f \frac{S_w}{A_z}$.

Equations (65) to (67) hold for the complete wing when streamwise upper surfaces are added, if S_w is interpreted as the combined surface area of the upper and lower surfaces.

To the list of parameters which determine the inviscid performance (M, C_L, λ and ξ) have now been added C_f and S_w/A_z to account for the effects of viscosity. A value of C_f, the average skin-friction coefficient, is difficult to assess accurately. However in many cases it is sufficient to assume a constant value. With this assumption the reduction of C_{Df} depends on reducing S_w/A_z. For a caret wing the value of S_w/A_z depends on the ratio of semi-span to length (s/l). In the next Section, using this as a parameter, values of S_w/A_z for the caret wing and W-wing are compared.

7. *The Ratio of Wetted Area to Plan Area.*

For the caret wing from Ref. 3,

$$\frac{S_w}{A_{zo}} = \left[1+\left(\frac{\tan\sigma}{s/l}\right)^2\right]^{\frac{1}{2}} + \left[1+\tan^2\delta+\left(\frac{\tan\sigma-\tan\delta}{s/l}\right)^2\right]^{\frac{1}{2}} \tag{68}$$

where S_w is the surface area excluding the base. For δ small this reduces to

$$S_w/A_{zo} = 2\sec\phi_o \tag{69}$$

where $\tan\phi_o = z_3/y_3$, and ϕ_o is usually referred to as the anhedral angle of the wing. Also for the caret wing

$$\frac{s}{l} = \frac{\tan\sigma}{\tan\phi_o}. \tag{70}$$

For the conical W-wing with δ small

$$\frac{S_w}{A_z} = 2\sec\phi + \frac{z_2}{y_3}. \tag{71}$$

The first term comes from the 'wing' at anhedral ϕ, as in equation (69); the z_2/y_3 term comes from the extra area of the body. The value of s/l can be written, using equation (3), as

$$\frac{s}{l} = \frac{y_3}{x_3} = \frac{y_3\tan\sigma}{z_3\cos\lambda + y_3\sin\lambda} \tag{72}$$

i.e.

$$\frac{s}{l} = \frac{\tan\sigma}{\cos\lambda\tan\phi+\sin\lambda}$$

$$= \frac{\tan\sigma\cos\phi}{\sin(\phi+\lambda)}. \tag{73}$$

For equal s/l from equations (70) and (73)

$$\frac{\tan\phi}{\tan\phi_o} = \frac{\sin\phi}{\sin(\phi+\lambda)}. \tag{74}$$

Hence the anhedral of the caret wing for a particular s/l, will be more extreme than that of the W-wing. This compensates in part for the extra surface area of the body, given by the z_2/y_3 term of equation (71).

a maximum at about $C_L = 0{\cdot}04$. For values of $\xi = \lambda =$ constant (> 0), larger values of L/D are obtainable at higher C_L.

The maximum value of L/D is given by

$$\frac{d}{dC_L}\left(\frac{D}{L}\right) = 0\,. \tag{77}$$

From equation (67),

$$\frac{D}{L} = \frac{C_{Do}}{C_L}\frac{\cos\xi}{\cos(\xi-\lambda)} + \frac{C_{Df}}{C_L}\,. \tag{78}$$

Hence the maximum L/D is given by

$$\frac{\cos\xi}{\cos(\xi-\lambda)}\frac{d}{dC_L}\left(\frac{C_{Do}}{C_L}\right) + \frac{C_{Do}}{C_L}\frac{d}{dC_L}\left(\frac{\cos\xi}{\cos(\xi-\lambda)}\right) + \frac{d}{dC_L}\left(\frac{C_{Df}}{C_L}\right) = 0\,. \tag{79}$$

The equation can be simplified when its second term is small. The magnitudes of the terms are investigated successively. From equation (8),

$$\frac{d}{dC_L}\left(\frac{C_{Do}}{C_L}\right) = \frac{C_{Do}}{C_L^2}\left(1 + \frac{C_L}{2-C_L} - \frac{2\beta_\infty^2}{4\beta_\infty^2 - (\gamma+1)C_L M_\infty^2} + \frac{2}{4+(\gamma+1)C_L M_\infty^2}\right) \tag{80}$$

$$= \frac{C_{Do}}{C_L^2} f(C_L)\,. \tag{81}$$

The function f is plotted in Fig. 17 for various Mach numbers.

Let the variation of C_{Df} with C_L be written as a Taylor series

i.e.

$$C_{Df}(C_L) = C_{Df}(0) + C_L\left(\frac{dC_{Df}}{dC_L}\right)_o + \frac{C_L^2}{2}\left(\frac{d^2C_{Df}}{dC_L^2}\right)_o + \ldots. \tag{82}$$

Then

$$\frac{d}{dC_L}\left(\frac{C_{Df}}{C_L}\right) = -\frac{C_{Df}(0)}{C_L^2} + \frac{1}{2}\left(\frac{d^2C_{Df}}{dC_L^2}\right)_o + \ldots. \tag{83}$$

$$\sim -\frac{C_{Df}(0)}{C_L^2} \tag{84}$$

for the values of C_L of interest. Then equation (79) can be written

$$\frac{\cos\xi}{\cos(\xi-\lambda)}f + C_L\frac{d}{dC_L}\left(\frac{\cos\xi}{\cos(\xi-\lambda)}\right) - \frac{C_{Df}(0)}{C_{Do}} = 0\,. \tag{85}$$

If the variation of λ and ξ with C_L is not large, the second term (with C_L equal to 0·1 or less) is small compared with $\frac{\cos \xi}{\cos (\xi - \lambda)} f$ and hence

$$\frac{\cos \xi}{\cos (\xi - \lambda)} f \approx \frac{C_{Df}(0)}{C_{Do}}$$

i.e.

$$C_{Dp} \approx \frac{C_{Df}(0)}{f}. \tag{86}$$

Then substituting this in equation (67)

$$\left(\frac{L}{D}\right)_{\max} = \frac{L}{D_p} \frac{1}{1 + f\, C_{Df}/C_{Df}(0)}. \tag{87}$$

The value of C_{Df}/C_{Df} (0) for a turbulent boundary layer on the compression surface of an inclined flat plate, has been calculated assuming no heat transfer[13] and a typical Reynolds number (*see* Fig. 18). For a W-wing with a streamwise upper surface, $C_{Df}/C_{Df}(0)$ for the wing will differ from unity by 1/2 to 2/3 of the values of Fig. 19. Hence the factor $f\, C_{Df}/C_{Df}(0)$ of equation (87), is usually close to unity, and we can write

$$\left(\frac{L}{D}\right)_{\max} \approx \frac{1}{2} \frac{L}{D_p} \tag{88}$$

with

$$C_{Dp} \approx C_{Df}. \tag{89}$$

This is similar to the well known result that, when C_D can be expressed as

$$C_D = C_1 + C_2 C_L^2 \tag{90}$$

with C_1 and C_2 constant, then $(L/D)_{\max}$ is given by $C_1 = C_2 C_L^2$.

From equation (67) C_{Dp} can be expressed as

$$C_{Dp} = \frac{C_L^2}{K} \frac{\cos \xi}{\cos (\xi - \lambda)} \tag{91}$$

where $K = \frac{C_L^2}{C_{Dpo}}$, (*see* Fig. 5). Then

$$\left(\frac{L}{D}\right)_{\max} = \left(\frac{K}{4\, C_{Df}} \frac{\cos (\xi - \lambda)}{\cos \xi}\right)^{\frac{1}{2}} \tag{92}$$

and is plotted against C_{Df} at $M = 4$, for various $\xi = \lambda$ in Fig. 19. The maximum value of $(L/D)_{max}$ is also shown using the upper allowable limit of ξ given in Fig. 15. This is an upper limit to the performance

that can be obtained with W-wings at $M = 4$.

If we write C_{Df} as $C_f S_w/A_z$, then if $\lambda = \xi$,

$$\left(\frac{L}{D}\right)_{\max} = \left(\frac{K}{4C_f}\right)^{\frac{1}{2}} \left(\frac{\sec \xi}{S_w/A_z}\right)^{\frac{1}{2}} \tag{93}$$

Fig. 19 can now be given a different interpretation by replacing C_{Df} along the abscissa by C_f and the constant parameter along the curves (sec ξ) by sec $\xi/(S_w/A_z)$. Then for given C_f, to improve the performance it is necessary to increase sec ξ more than the wetted area to planform ratio. This gives a quantitative estimate of the prospects of improving the performance.

9. *Conclusions.*

The flow through a plane inclined shock wave can be used to produce a lifting surface with an exactly known inviscid flow, and better inviscid performance than that of the two-dimensional wedge. The shock wave must be skew to the flow; the compression surface has single curvature and no vertical plane of symmetry.

A complete analysis of shapes supporting plane skew shock waves is presented. It is found that the optimum performance of such compression surfaces with supersonic trailing edges depends on a similarity parameter $C_L^{\frac{1}{2}} M_\infty^2/\beta_\infty$ (Fig. 15). Small values of the parameter give much larger values of lift to drag ratio than that of the two-dimensional wedge (which is the value given by a caret wing).

A relatively simple configuration, here termed a W-wing, can be formed from a pair of these compression surfaces with a partly common leading edge. The shape has in effect a central body below a swept wing and demonstrates an advantageous interference of the body on the wing. Restrictions on compression-surface shape from the single curvature of the surface can be relaxed by using the two-dimensional flow about curved wedges. Although these wings are not immediately representative of practical aircraft configurations, they can be used to indicate the distribution of volume and wing position for obtaining favourable interference when the wing supports an attached shock wave.

Viscous drag tends to be high, because the shapes have a large ratio of wetted area to plan area. For hypersonic speeds ($M > 5$) where the inviscid improvement over a two-dimensional wedge is small, the high viscous drag puts the W-wings at a disadvantage as compared with flat-bottomed configurations (though not as compared with caret wings). At high supersonic speeds ($3 < M < 5$) the inviscid improvement is more marked and a gain in performance, including viscosity, over that of the two-dimensional wedge, and hence over that of flat-bottomed shapes, can be shown.

The optimum lift to drag is found to be obtained when the pressure drag is approximately equal to the viscous drag.

LIST OF SYMBOLS

a, b, c	Defined in equation (19)
A_y	$\int_S \mathbf{y} \cdot \mathbf{dS}$
A_z	Plan area defined by equation (1)
B	Cot $(\sigma - \delta)$
C_D, C_S, C_L	Force coefficients, with A_z as reference area, in the x, y and z directions
C_{Dp}	Pressure drag
C_p	Pressure coefficient behind shock wave
f	Defined in equation (81)
K	C_L^2/C_{Dpo}
M_∞	Free-stream Mach number
P	A point in the flow
S	The compression surface
S_w	Wetted area
s/l	Semi-span to length ratio
x, y, z	Free-stream axes, shown in Fig. 1.
X_o, Y_o, Z_o	X, Y, Z axes with $\lambda = 0$
X, Y, Z	Rectangular axes, positive X streamwise behind the shock wave, Y in the shock wave, and positive Z in the free stream (*see* Fig. 3)
$\mathbf{y}$	Unit vector in y direction
$\mathbf{z}$	Unit vector in z direction
β	$\sqrt{M^2-1}$ behind the shock wave
β_∞	$\sqrt{M_\infty^2-1}$
δ	Angle of flow deflection on passing through the shock wave
λ	Angle between a streamwise plane perpendicular to the shock wave, and the x, z plane
ξ	$\tan^{-1}(A_{yo}/A_{zo})$ (equation (4))
σ	Shock wave inclination to free stream
ϕ	Anhedral angle $\tan^{-1}(z_3/y_3)$
0	$\lambda = 0$
1	Nose, co-ordinates (0, 0, 0)
2 and 3	Wing tips
4	Point of intersection of nose streamline with trailing edge
v	Viscous term included
f	Skin friction

REFERENCES

No.	*Author(s)*	*Title, etc.*
1	T. R. F. Nonweiler . .	Aerodynamic problems of space vehicles. *Jl. R. Aeronaut. Soc.* 63 (585) Sept. 1959.
2	T. R. F. Nonweiler . .	Delta wings of shapes amenable to exact shock wave theory. A.R.C. 22,644 March 1961. *Jl. R. Aeronaut Soc. 67* (625) Jan. 1963.
3	D. Kuchemann . .	Hypersonic aircraft and their aerodynamic problems. *Advances in Aeronautical Science* Vol. 6 1965.
4	P. L. Roe	Some exact calculations of the lift and drag produced by a wedge in supersonic flow, either directly or by interference. A.R.C. R. & M. 3478, Aug. 1964.
5	V. V. Keldysh . .	Exact solutions for wings having one and two plane shock waves. *Inzhenernyi Zhurnal* 1 (1961) 3, pp 22-39. R.A.E. Lib. Trans. No. 1044 Sept. 1963.
6	Ames Research Staff . .	Equations, Tables, and Charts for compressible flow. N.A.C.A. Report 1135, 1953.
7	A. J. Eggers and C. A. Syvertson . .	Aircraft configurations developing high lift-drag ratios at high supersonic speeds. N.A.C.A./T.I.B. 5007. N.A.C.A. R.M. A55 L.O.S., 1956, A.R.C. 18632.
8	J. Pike	Minimum drag surfaces of a given lift which support two-dimensional flow fields A.R.C. R. & M. 3543, Sept. 1966.
9	G. L. Grodzovskii . .	Useful interference of a wing fuselage at hypersonic speeds *Izv. a. n. SSSR. Otd. Tekh. n. Mechanika i. Mashinstroeme* No. 1 pp 170-173, 1959.
10	D. A. Babeav	Numerical solution of the problem of supersonic flow past the lower surface of a delta wing. *Zhurnal Vychislitel 'noi Mathematiki i Mathematicheskoi Fiziki* 2, No. 6, 1086-1101, Nov. 1962. *A.A.I.A. Journal*, Vol. 1, No. 9, Sept. 1963.
11	J. G. Jones and B. A. Woods . .	The design of compression surfaces for high supersonic speeds using conical flow fields. A.R.C. R. & M. 3539 March 1963.
12	J. V. Becker	Studies of high lift/drag ratio hypersonic configurations. U.S.A. A.I.A.A. Paper 64-551, 1964.8.
13	K. G. Smith	Methods and charts for estimating skin-friction drag in wind-tunnel tests with zero heat transfer. A.R.C. C.P. 824. Aug. 1964.

APPENDIX A

The Trailing-Edge Surface

Angle ξ represents an important parameter in the performance of generalised Nonweiler wings. It is purely a geometrical parameter depending on the trailing-edge shape (*see* equations (4) and Fig. 4). In order to find simple classes of wings with constant ξ, the concept of a trailing-edge surface is introduced. This is a curved surface which passes through the downstream limit (i.e. the trailing edge) of the stream surface (Fig. 20). More exactly, it is a semi-infinite surface with a boundary $P_2 P_3$ in the shock wave, such that it prescribes a trailing edge to any stream surface with a leading edge which ends in this boundary. The supersonic trailing-edge condition can be given as a property of the trailing-edge surface. Consider a trailing-edge surface such that no streamline crosses it more than once, and the surface is everywhere locally supersonic. Then no downstream influence can propagate across the surface and any trailing edge on such a surface must necessarily be supersonic. Further any supersonic trailing edge will have at least one such surface through it, for the upstream limit of influence of the downstream Mach cones from trailing-edge points form such a surface. Hence all supersonic trailing edges are defined by the class of trailing-edge surfaces which are locally supersonic.

A parallel region of flow such as $P_1 P_2 P_3 P_4$ (e.g. in Fig. 7) is bounded upstream by the shock wave downstream by the supersonic trailing-edge surface, and elsewhere by the stream surface. Consider this parallel flow region divided into n streamtubes such that the trailing edge surface may be considered plane for any one of them, then

$$A_{zo} = \sum_{r=1}^{r=n} (A_{zo})_r \tag{94}$$

$$A_{yo} = \sum_{r=1}^{r=n} (A_{yo})_r \tag{95}$$

Hence

$$\tan \xi = \frac{A_{yo}}{A_{zo}} = \sum_{n=1}^{n=r} \frac{(A_{zo})_r}{A_{zo}} \tan \xi \tag{96}$$

where

$$\sum_{r=1}^{r=n} \frac{(A_{zo})_r}{A_{zo}} = 1 . \tag{97}$$

The maximum of $\tan \xi_r$ with only a locally supersonic trailing edge restriction, will give an orientation of the trailing-edge surface. The 'locally supersonic' condition depends on flow properties. These are constant over the trailing-edge surface. Hence for any r, $\tan \xi_r$ has the same maximum value at the same orientation. Hence from equations (96) and (97), $\tan \xi$ has this same maximum, with a surface of constant orientation. Hence plane trailing-edge surfaces include a surface which gives the maximum value of $\tan \xi$.

For a particular plane trailing-edge surface the ratio of $(A_{yo})_r$ to $(A_{zo})_r$ (i.e. $\tan \xi_r$) is a constant. Hence from equations (96) and (97), ξ is constant for any compression surface with its trailing edge of this trailing-edge surface. Hence given a plane shock wave and a plane trailing-edge surface the inviscid performance is independent of the shape of the compression surface.

APPENDIX B

The Volume Coefficient

In Section 8 it is indicated how a C_L may be obtained for optimum lift to drag ratio. *Via* equation (2) and the oblique shock wave relationships[6] C_L determines the angle of flow deflection (δ). For δ constant over the compression surface, the volume for any wing with a streamwise upper surface may easily be evaluated
i.e.

$$V = V_o = \frac{\tan \delta}{} \int_{Y_2}^{Y_3} x^2 \, dY \tag{98}$$

where x is the chord at any Y value.

This volume may not be as large as the volume required for the configuration. It is of interest then to compare the volume of the W-wing with that of the caret wing.

For the conical wing with a plane trailing-edge surface (e.g. Fig. 7), x is linear with Y and

$$V = \frac{\tan \delta}{3} x_4^2 \left(\frac{Y_3 - Y_2}{2} \right). \tag{99}$$

For the caret wing this reduces to

$$V_o = \frac{\tan \delta}{3} x_4^2 s \,. \tag{100}$$

Introducing a non-dimensionalised volume

$$\tau = \frac{V}{A^{3/2}} \tag{101}$$

i.e.

$$\tau = \frac{V}{s^{3/2} x_4^{3/2}} \,. \tag{102}$$

Then

$$\tau_o = \frac{\tan \delta}{3} \frac{1}{\sqrt{s/x_4}} \,. \tag{103}$$

For the W-wing,

$$\frac{Y_3 - Y_2}{S} = \frac{Y_3 - Y_2}{y_3 - y_2} \frac{x_4}{x_4} = \frac{A_{zo}}{A_z} = \frac{\cos \xi}{\cos (\xi - \lambda)} \,. \tag{104}$$

Hence from equations (102) and (104)

$$\tau = \frac{\tan \delta}{3} \frac{\cos \xi}{\cos (\xi - \lambda)} \frac{1}{\sqrt{s/x_4}}. \tag{105}$$

From equations (11), (103) and (105), for either a caret wing or a W-wing

$$\tau \frac{L}{D_p} = \tau_o \left(\frac{L}{D_p} \right)_o = \frac{1}{3\sqrt{s/x_4}}. \tag{106}$$

Hence for wings of the same L/D_p, and s/x_4 the τ is constant.

The spanwise distribution of volume is very dependent on λ (e.g. Fig. 8), so that a large proportion of the volume can be concentrated in a central body. The volume can easily be increased by extending this body downstream, as is shown in Fig. 8c, to give a larger value of τ while making little difference to the performance.

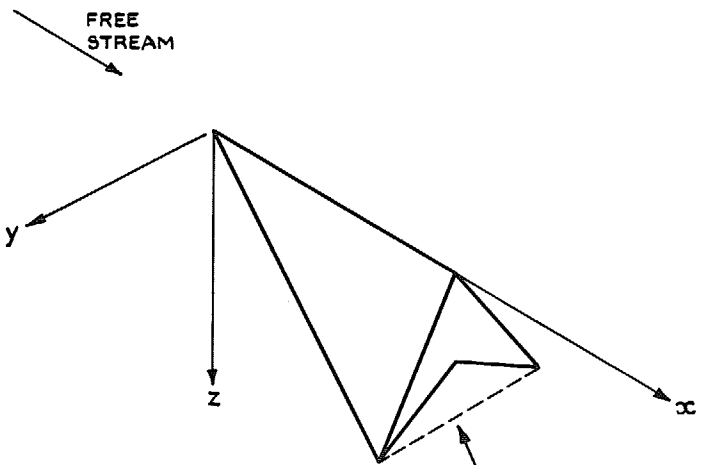

FIG. 1a. A caret wing.

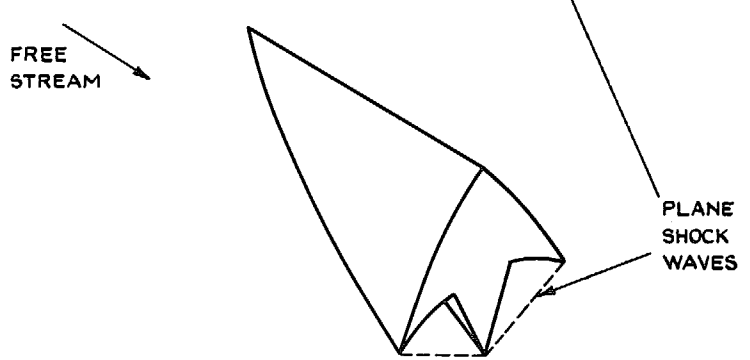

FIG. 1b. A generalised 'W'-Nonweiler wing.

FIG. 1 A caret wing and a 'W'-Nonweiler wing.

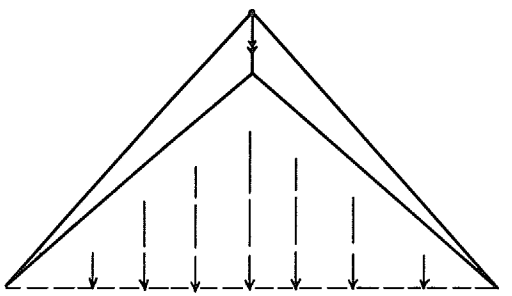

FIG. 2a. Caret wing.

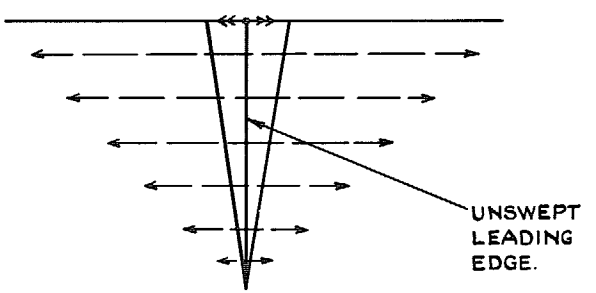

FIG. 2b. Interference wing.

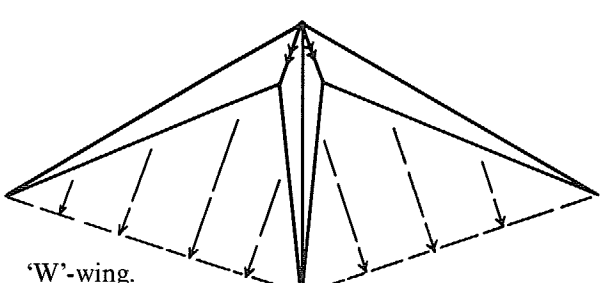

FIG. 2c. 'W'-wing.

FIG. 2. Front view of various wings based on two-dimensional flow fields showing 'local' flow direction.

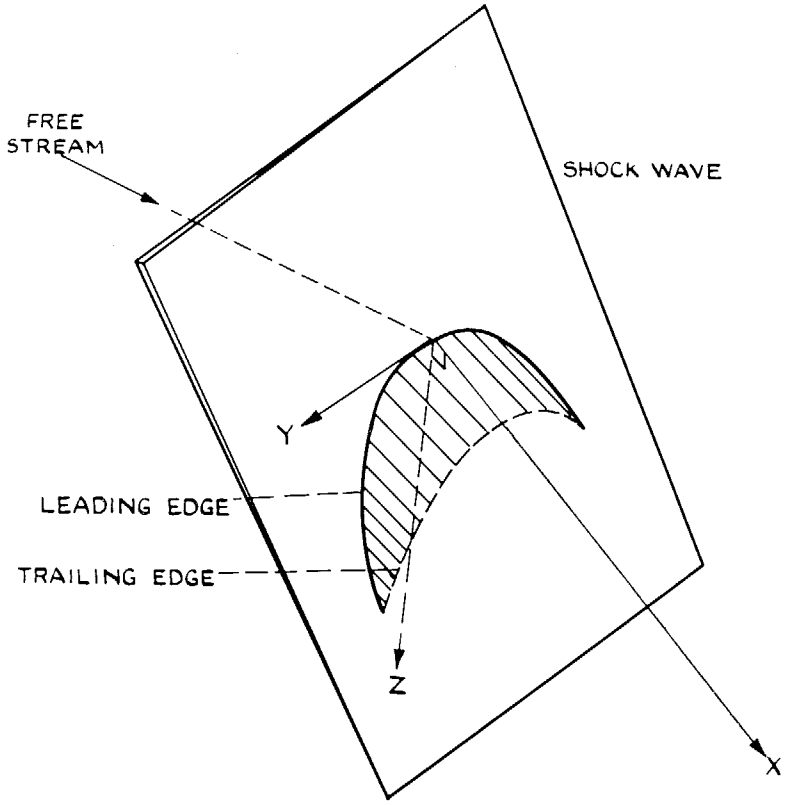

FIG. 3. The stream surface through a leading edge on a plane shock wave.

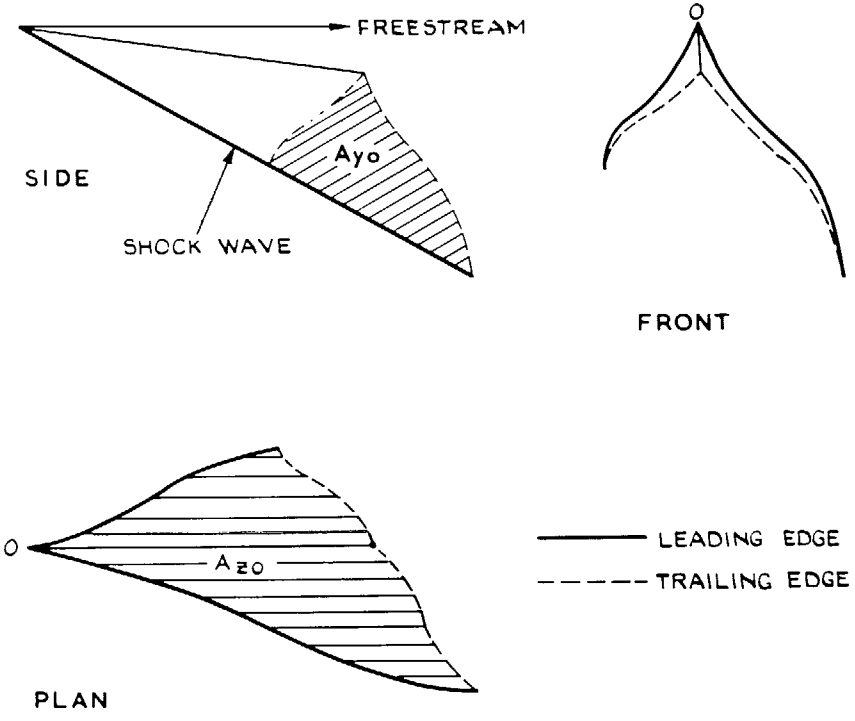

FIG. 4. The projected areas A_{yo} and A_{zo}.

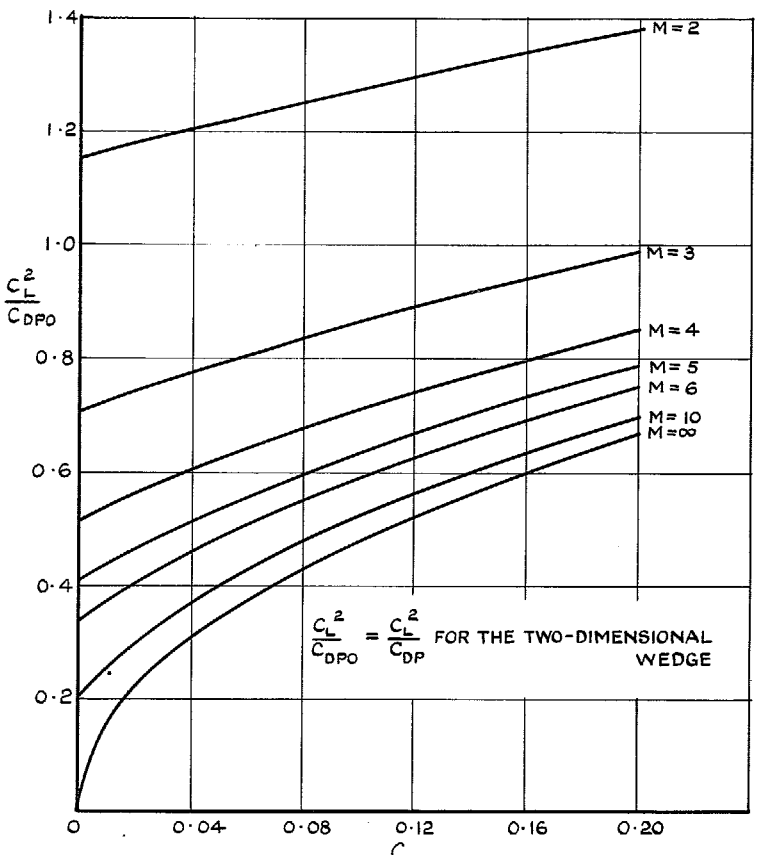

FIG. 5. Values of C_L^2/C_{Dpo}.

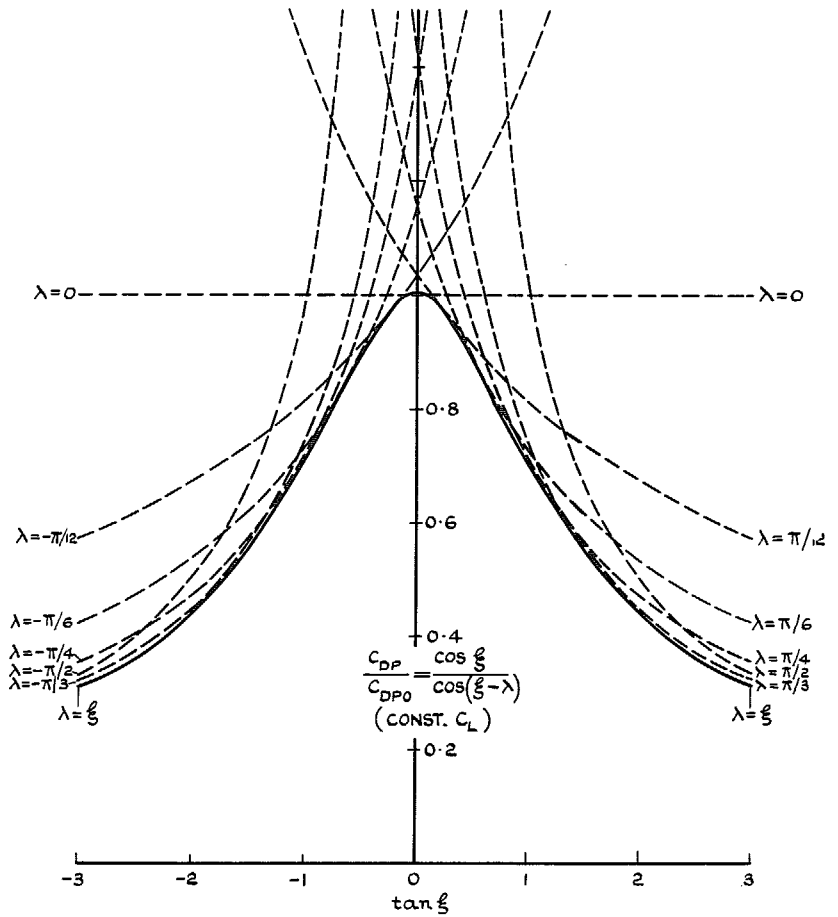

FIG. 6. The function $\cos\xi/\cos(\xi-\lambda)$.

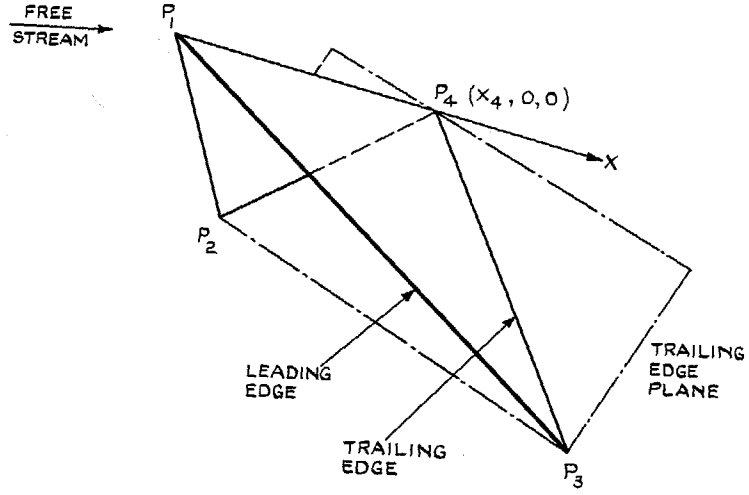

FIG. 7. Plane trailing-edge surface.

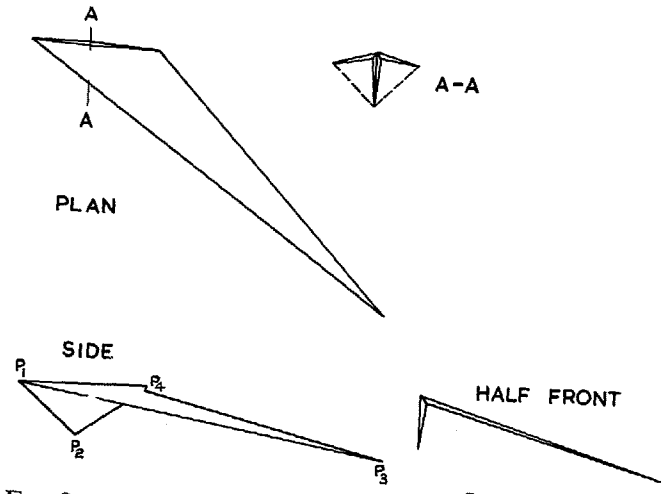

FIG. 8a. $M_\infty = 2, \delta = 4°, C_L = 0{\cdot}088, \frac{L}{D_p} = 20.$

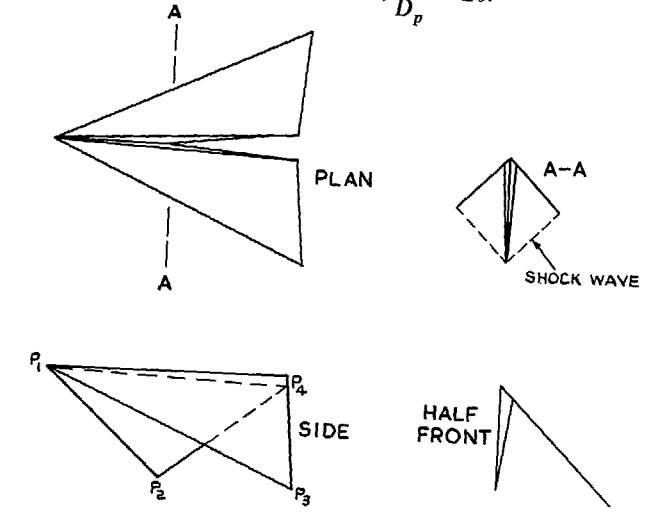

FIG. 8b. $M_\infty = 2, \delta = 4°, C_L = 0{\cdot}088, \frac{L}{D_p} = 20.$

FIG. 8. Examples of 'W'-wings.

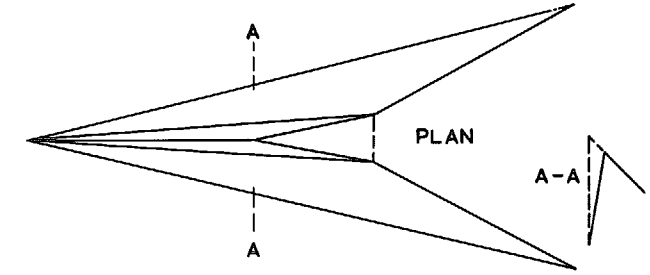

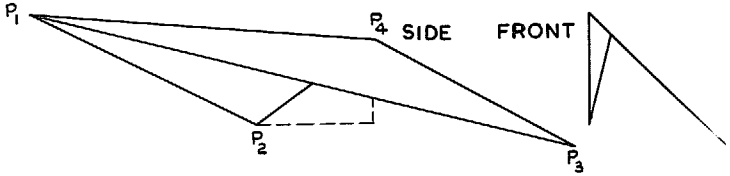

FIG. 8c. $M = 4$, $\delta = 6^o$, $C_L = \cdot 069$, $\xi = \lambda = \frac{\pi}{4}$

$L/D_p = 13{\cdot}3$.

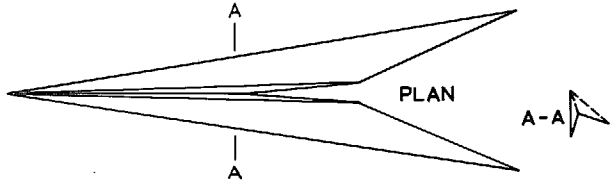

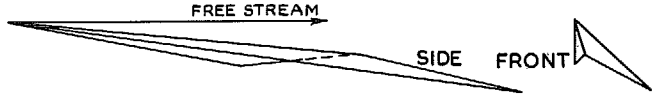

FIG. 8d. $M = 10$, $\delta = 6^o$, $C_L = 0{\cdot}038$, sec $\xi = 1{\cdot}05$,

$$\frac{L}{D_p} = 10$$

FIG. 8 (*cont.*) Examples of 'W'-wings.

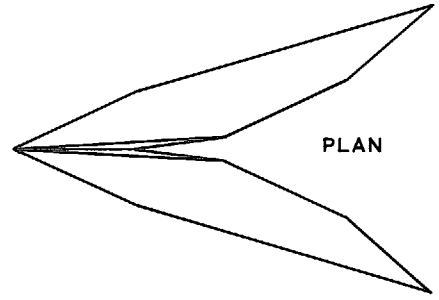

FIG. 9a. $M = 4$, $\delta = 6°$, $C_L = 0{\cdot}069$, sec ξ = sec $\lambda = 1{\cdot}25$,

$$\frac{L}{D_p} = 11{\cdot}8$$

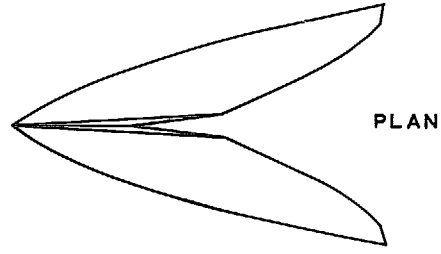

FIG. 9b. $M = 4$, $\delta = 6^o$, $C_L = \cdot 069$, sec ξ = sec $\lambda = 1{\cdot}25$,

$$\frac{L}{D_p} = 11{\cdot}8.$$

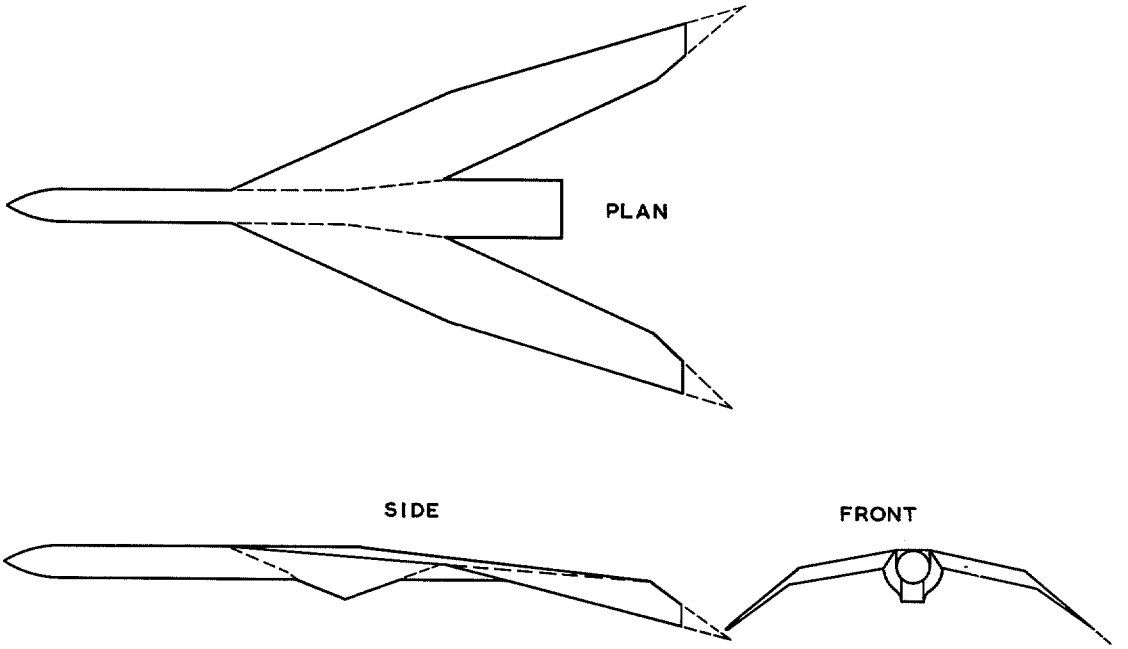

FIG. 10. Compression surfaces on design at $M = 4$ arranged about an arbitary fuselage.

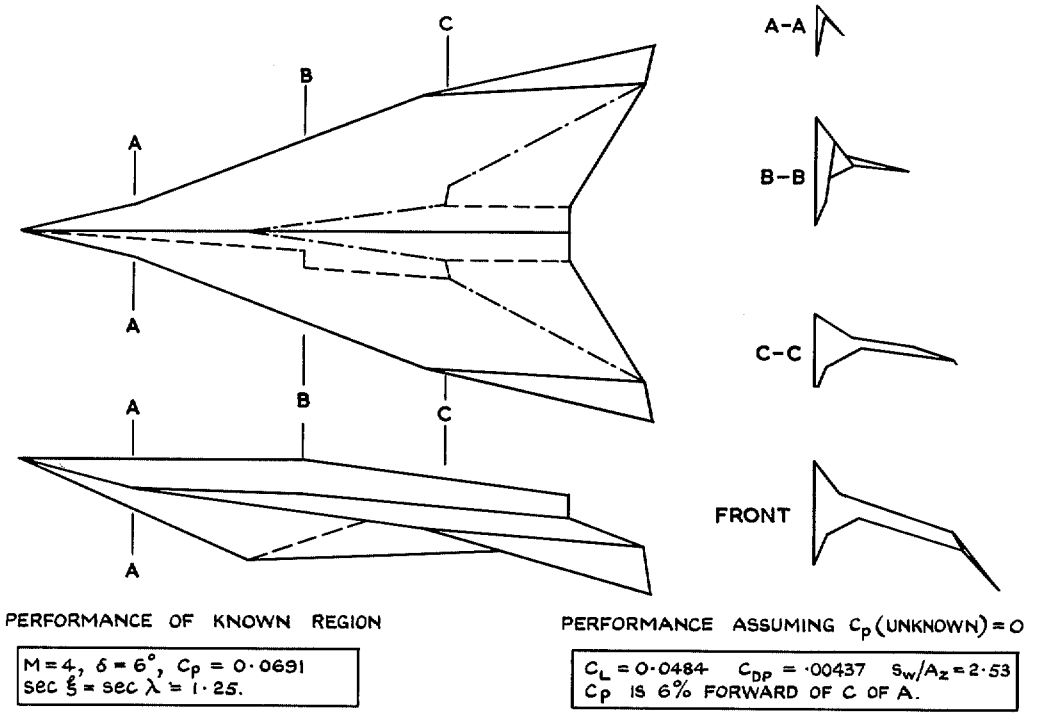

FIG. 11. An example of an extended 'W'-wing.

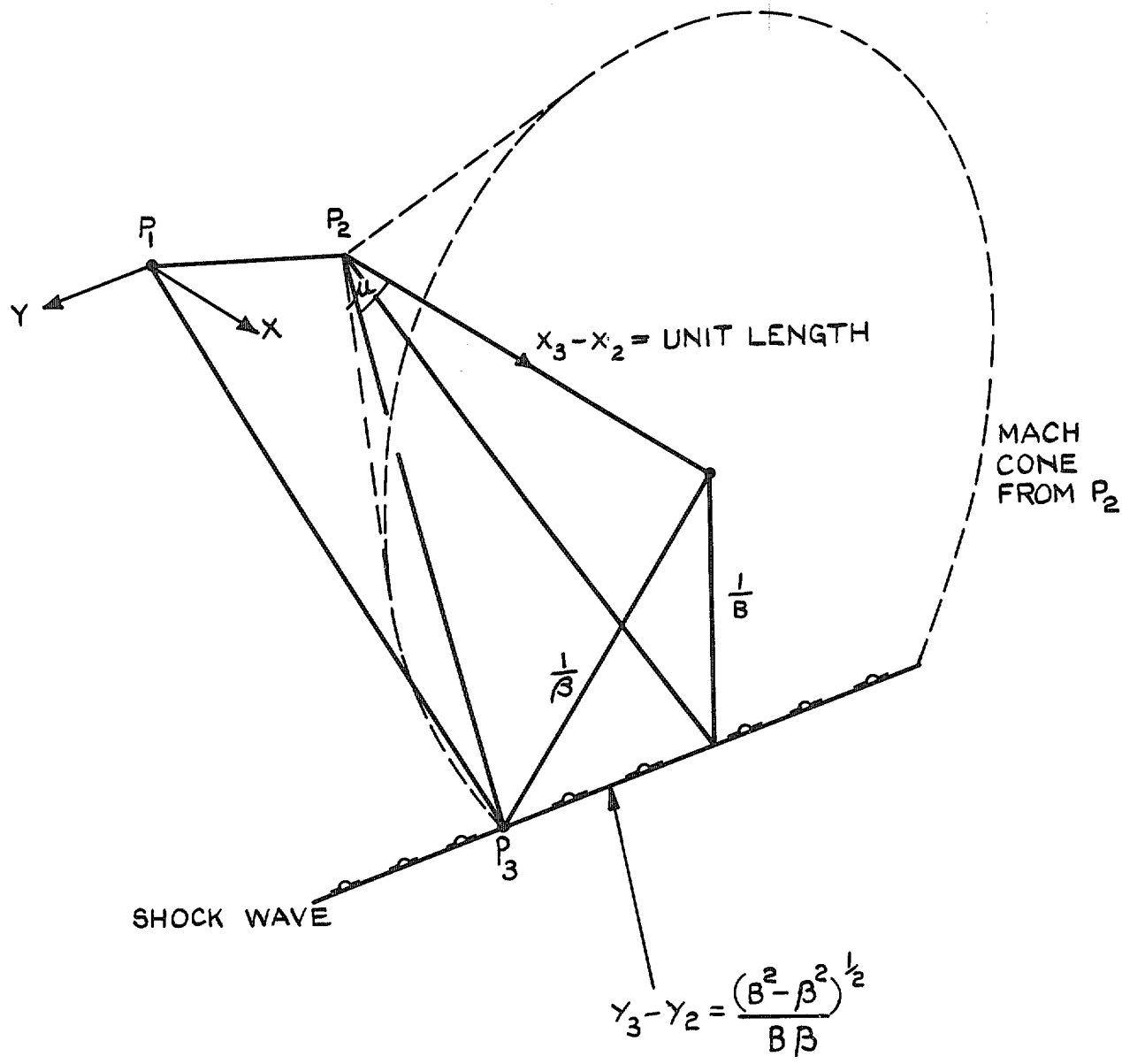

FIG. 12. The downstream Mach cone from P_2.

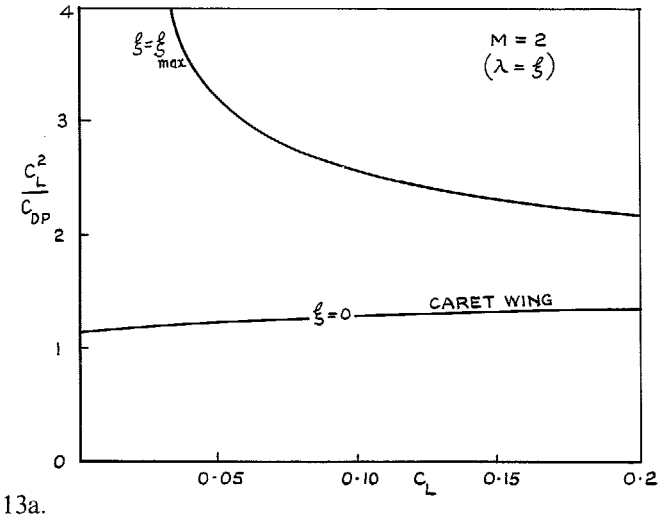

FIG. 13a.

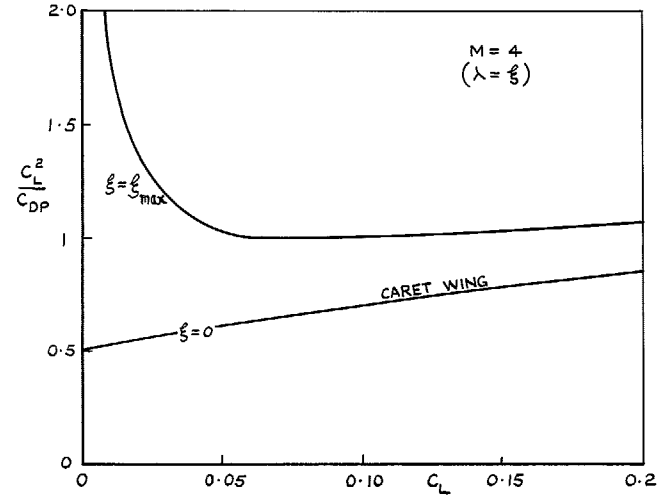

FIG. 13b.

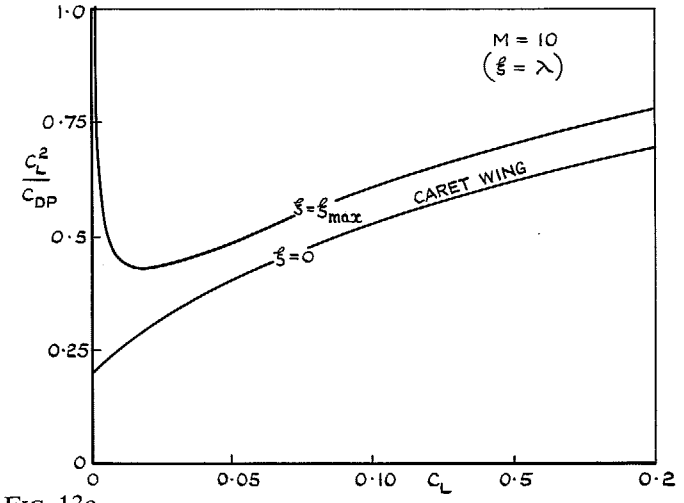

FIG. 13c.

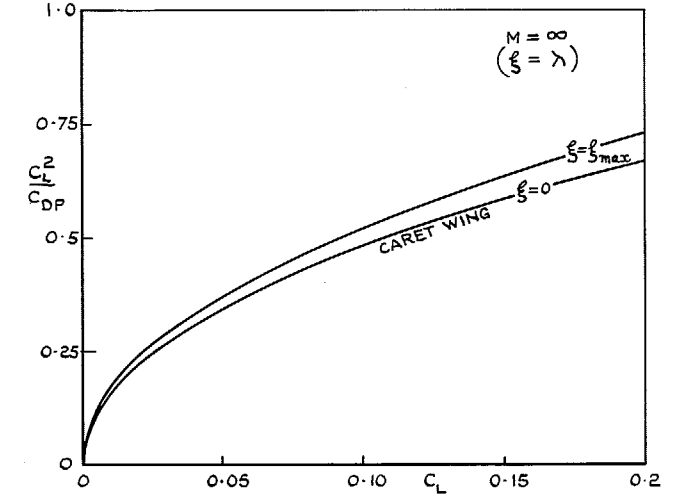

FIG. 13d.

FIG. 13. The performance of optimum 'W'-Nonweiler wings (no viscous drag).

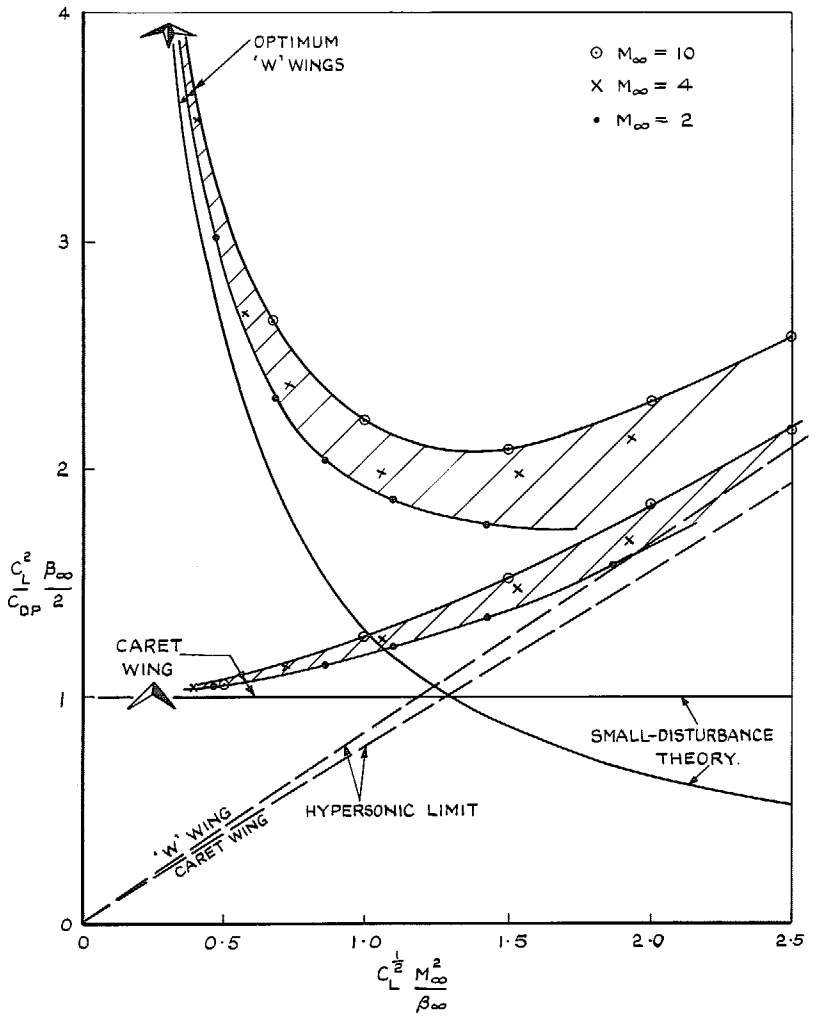

FIG. 14. Inviscid performance of plane-shock wings.

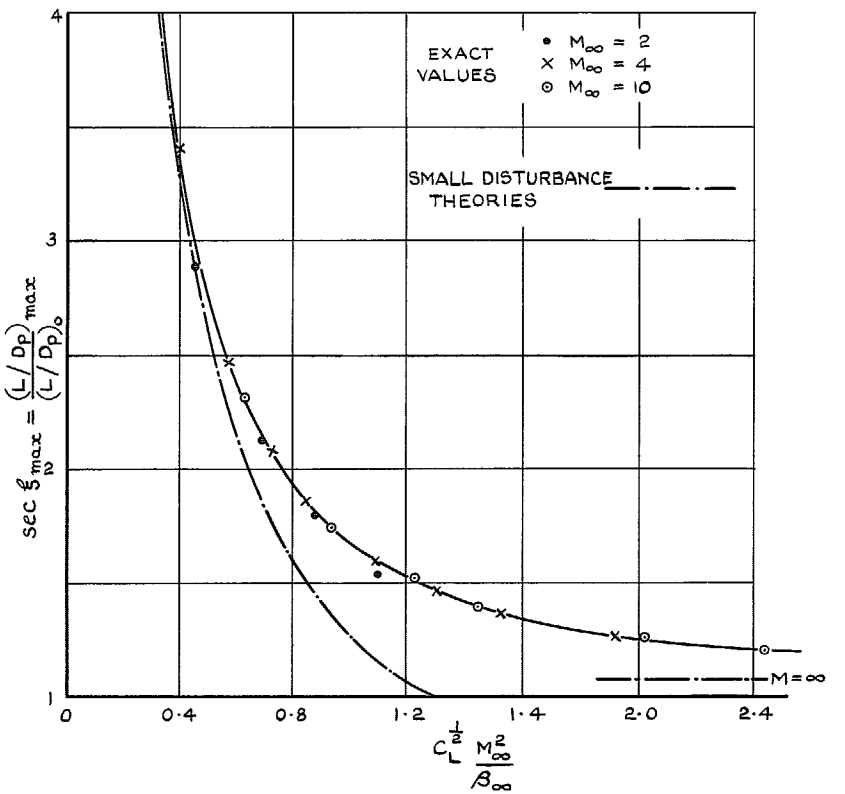

FIG. 15. Collapsed plot of optimum performance improvement.

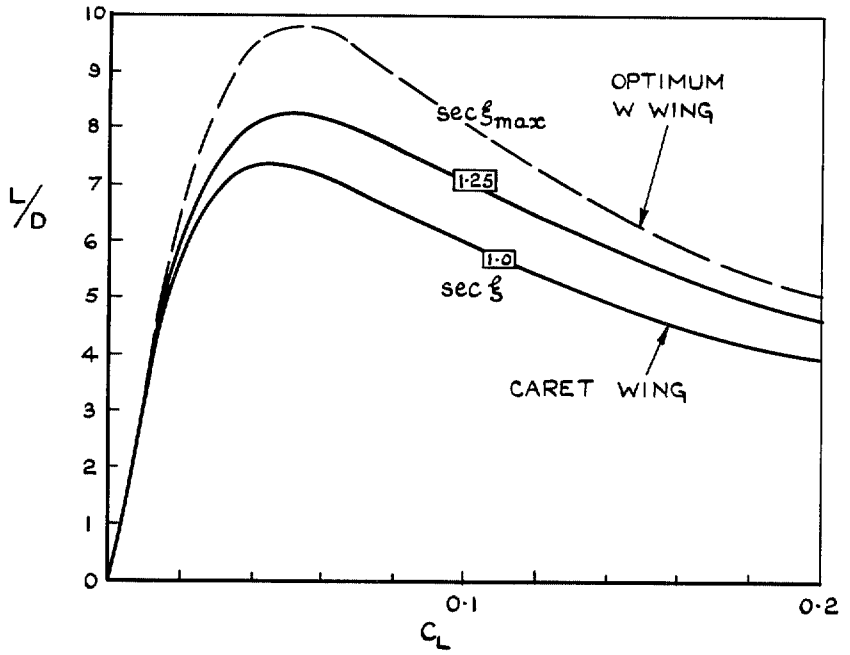

FIG. 16. The performance of 'W'-wings at $M = 4$ with $C_{Df} = 0{\cdot}0028$.

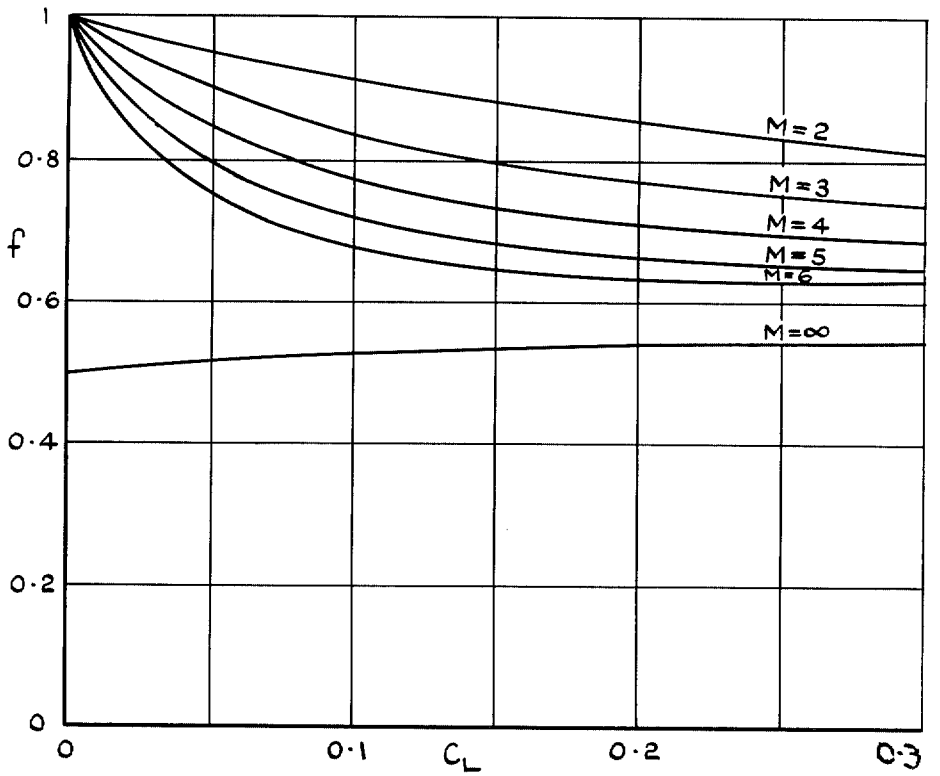

FIG. 17. The value of f.

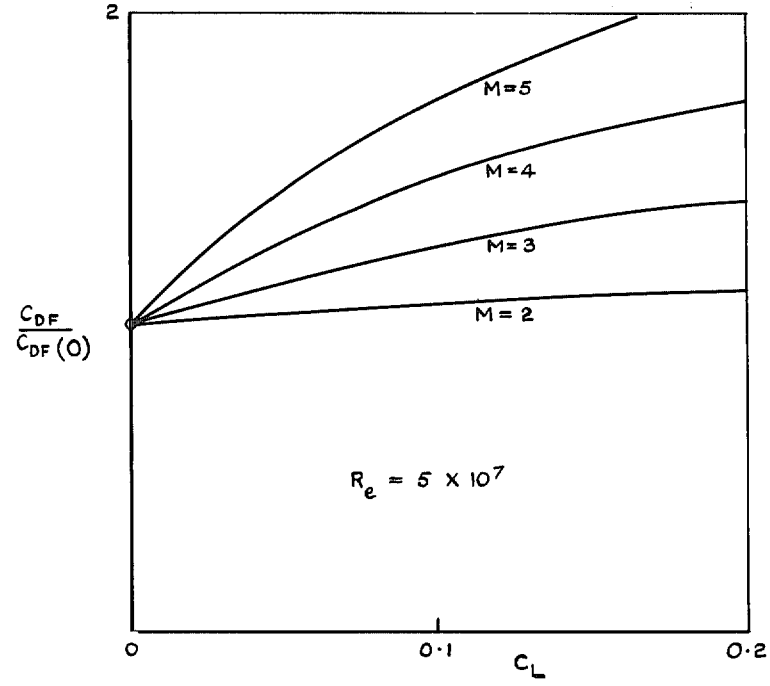

FIG. 18. $C_{Df}/C_{Df}(0)$ for the compression surface of an inclined flat plate.

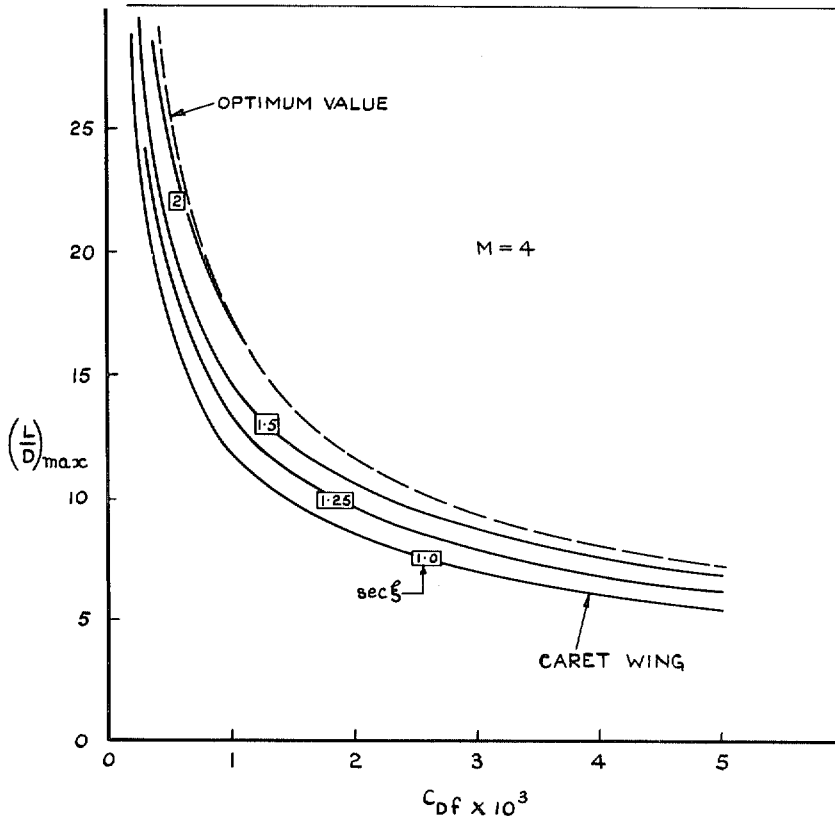

FIG. 19. $(L/D)_{\max}$ for various values of $\xi = \lambda$.

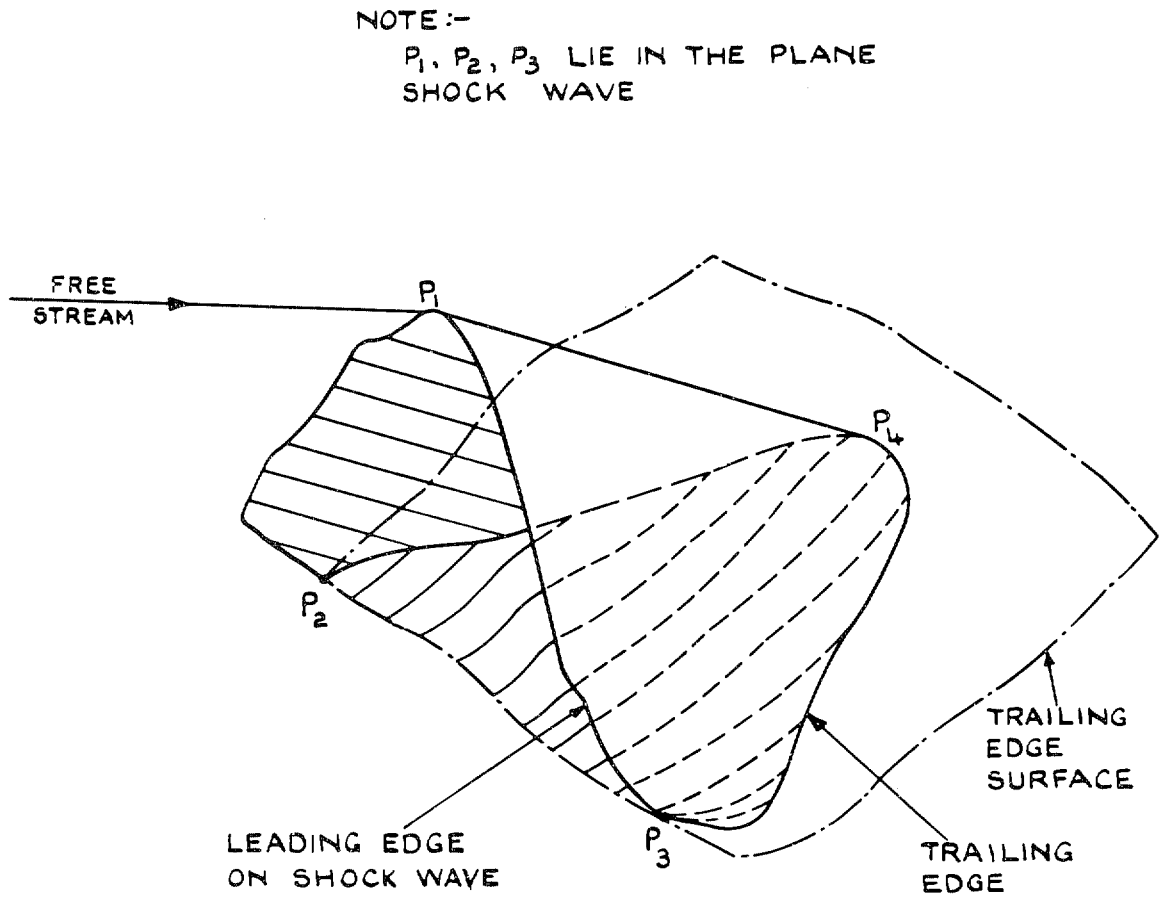

FIG. 20. Curved trailing-edge surface.

Printed in Wales for Her Majesty's Stationery Office by Allens Printers (Wales) Limited
Dd 146916 K5

Published by
HER MAJESTY'S STATIONERY OFFICE

To be purchased from
49 High Holborn, London WC1
13a Castle Street, Edinburgh EH2 3AR
109 St Mary Street, Cardiff CF1 1JW
Brazennose Street, Manchester M60 8AS
50 Fairfax Street, Bristol BS1 3DE
258 Broad Street, Birmingham 1
7 Linenhall Street, Belfast BT2 8AY
or through any bookseller

R. & M. No. 36

SBN 11 470323